머리 MR영상에서 자동화된 뇌영역 추출

Automated Brain Region Extraction Method in Head MR Image Sets

조동욱
충북과학대학 정보처리과

김태우
삼성종합기술원 메디컬응용팀

신승수
(주)시그마정보기술 연구소장

Dong-Uk Cho
Dept. of Information & Telecommunications, Chungbuk Provincial University of Science & Technology
Tae-Woo Kim
Medical Application Team, Samsung Advanced Institute of Technology
Seung-Soo Shin
Sigma Information Technology Lab. Manager

중심어 : automatic thresholding, brain region extraction, dual curve fitting, magnetic resonance image(MRI), morphological operations

요 약

본 논문은 인간 뇌의 가시화 및 해석을 위하여 단일 채널 MR영상에서 자동화된 뇌영역 추출 방법을 제안한다. 이 방법은 쌍곡선 적합을 이용한 자동 문턱치화와 3차원 형태학적 연산에 의하여 뇌 마스크 볼륨을 생성한다. 쌍곡선 적합은 MR영상의 히스토그램에 곡선을 적합할 때 오차를 줄일 수 있으며, 침식, 연결부위 레이블링, 최대특징 연산, 팽창 등 3차원 형태학적 연산은 문턱치화된 뇌 마스크로부터 생성된 정육각형 볼륨 마스크에 적용된다. 제안한 방법은 SPGR, T1, T2, PD MR영상 세트에서 뇌영역을 자동 추출할 수 있으며, 가장자리 슬라이스에도 적용 가능하고, 영상이 뇌 전체를 포함하지 않아도 된다. 실험에서 20 세트의 MR영상에 적용하여 수동 방법과 비교하여 0.97 이상의 유사도를 보였다.

Abstract

A novel automated brain region extraction method in single channel MR images for visualization and analysis of a human brain is presented. The method generates a volume of brain masks by automatic thresholding using a dual curve fitting technique and by 3D morphological operations. The dual curve fitting can reduce an error in curve fitting to the histogram of MR images. The 3D morphological operations, including erosion, labeling of connected-components, max-feature operation, and dilation, are applied to the cubic volume of masks reconstructed from the thresholded brain masks. This method can automatically extract a brain region in any displayed type of sequences, including extreme slices, of SPGR, T1-, T2-, and PD-weighted MR image data sets which are not required to contain the entire brain. In the experiments, the algorithm was applied to 20 sets of MR images and showed over 0.97 of similarity index in comparison with manual drawing.

I. Introduction

MR images are widely used to non-invasively examine a brain or body of a human. Segmentation of a brain region in MR images is an important step for visualization and volume analysis of regions of interest(ROI's). Many computer-assisted definitions of ROI's require segmentation of the whole brain from the head MR images, either because the whole brain is the ROI such as in Alzhiemer's studies or because automatic ROI extraction using statistical methods is made easier if the skull and scalp have been removed[1],[2].

Reported methods for automatic segmentation of the

brain region have used image processing techniques such as histogram analysis[3],[5],[7], morphological operations[4], anisotropic filtering[5], template matching[6],[7], etc. These methods can be applied to segmentation of the brain region of limited kinds of MR images. Brummer *et al.*[4],[5] use histogram analysis and morphology to generate 3D brain masks. This method misses brain tissue in extreme slices and includes nonbrain tissues in others[1]. Furthermore, thresholding is achieved by curve fitting with a Gaussian curve to the top-half of the intensity histogram. In many cases, the top-half of the histogram does not have a Gaussian curve as shown in Fig. 5. Snell *et al.*[6] use an active surface template to find the intracranial boundary in MRI volume of the head. The method used high-resolution isotropic 3D MRI data set to test his algorithm. Such MRI scans are generally not performed clinically. The method may fail for images that do not contain the entire brain[5,6]. The method of Atkins *et al.*[1] can work well on axially displayed multispectral sequences and on axial and coronal 3D T1-weighted SPGR sequences. Its performance depends on displayed slice types, which are generally axial, coronal, and sagittal. SPM[7] segments the images using the templates and the modified mixture model algorithm in the process of registration between MR images and PET images. After aligning the images containing the whole brain, one should determine the affine transformations that map between the images and the templates. Because the modified mixture model algorithm fit the weighted intensity distribution with a probability density function for each cluster, the algorithm can cause errors in extracting the brain region as shown in Fig. 5.

In this paper, we propose a novel technique for automatic segmentation of a brain region in single channel T1, T2, PD, and SPGR MR images for visualization and analysis. Our method can overcome weaknesses of above methods using automatic thresholding by *a dual* curve fitting and 3D morphological operations in a cubic volume of masks reconstructed from thresholded images. The automatic thresholding is improved by the dual curve fitting with two Gaussian curves to the histogram. The cubic volume of masks is generated from the head masks thresholded on MR images for the 3D morphological operations, including erosion, labeling of connected-components, max-feature operation, and dilation in 3D. The 3D morphological operations applied to the cubic volume of masks do not require a specific displayed type of slices or MRI data sets to contain the entire brain.

The proposed method assumes requirements as follows. 1) The volume of masks generated for a ROI can be represented as one connected-component volume. 2) The volume of masks of the ROI separated from the head MR images is the largest in the volumes labeled as connected-components. 3) Intensity distribution of the brain region can be partially modeled as a Gaussian curve. Generally, above three assumptions are acceptable for MR images of the brain for clinical and research purpose. Assumption 1) and 2) are acceptable because a ROI in the head is the largest connected-component area such as a cerebrum or cerebellum in MR images composed of several sequential slices. Assumption 3) is acceptable because the left and right part of the top-half of the histogram of the brain region in MR images can be modeled as a Gaussian curve, not always for the whole histogram.

II. Automatic Segmentation of a Brain Region

Our method for automatic segmentation of a brain region in MR images is composed of mask generation steps of head masks, initial brain masks, intermediate brain masks, and final brain masks as shown in Fig.1. The dual curve fitting for automatic thresholding is applied to the top-half of the histogram of a set of MR images to generate brain masks. The intermediate brain masks are generated by applying 3D morphological operations to a cubic volume of masks reconstructed from the initial brain masks.

1. Generation of head masks

Head masks are generated by removing a background noise using the method of Brummer *et al.*[4]. The method

based on the fact[11] that a MRI scanner gives a white noise with Gaussian distribution. Henkelman[12] proved a background noise of MR images to be Rayleigh distribution represented as Eq. (1),

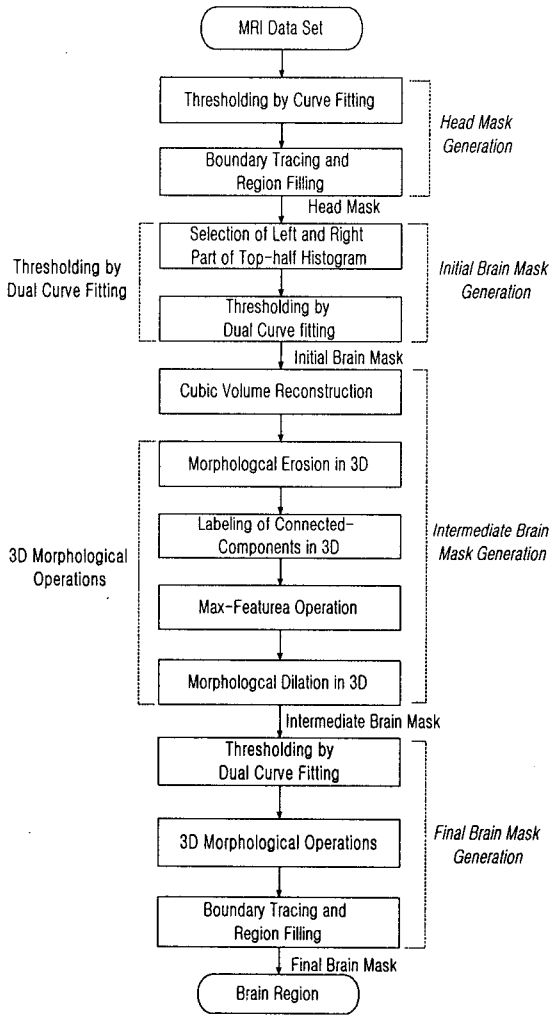

Fig. 1. Segmentation procedure of the proposed method for automatic segmentation of a brain region in MR images of a head.

$$p_N(f) = \frac{f}{\sigma^2}\exp\left(-\frac{f^2}{2\sigma^2}\right) \quad (1),$$

where f and σ is intensity and standard deviation of a noise, respectively. The threshold τ is determined[4,5] by minimizing ε_τ in Eq. (2),

$$\varepsilon_\tau = \sum_{f=0}^{\tau-1} g(f) + \sum_{f=\tau}^{\infty} r(f) \quad (2)$$

$$g(f) = h(f) - r(f) \quad (3)$$

where $h(f)$ is a histogram of MR images, and $r(f)$ is Rayleigh distribution function fitted to $h(f)$. Levenberg-Marquardt's fitting technique[10], a non-linear least square fitting, is used for automatic thresholding. A typical histogram distribution of T1, T2, and PD MR images, and an example of Rayleigh curve fitted to the histogram are shown in Fig. 2. A final head mask as shown in Fig. 3 is generated by boundary tracing and region filling[9] after removing background noise by morphological filtering[9].

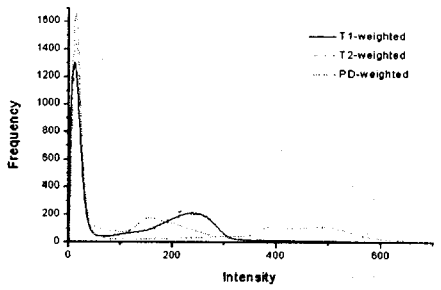

(a)

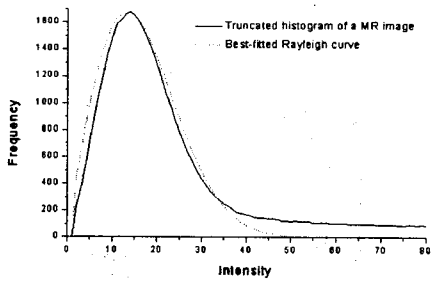

(b)

Fig. 2. (a) Typical histograms of T1-, T2-, and PD-weighted MR images, and
(b) Typical histogram of background noise and its best-fitted Rayleigh curve.

(a) The original image.

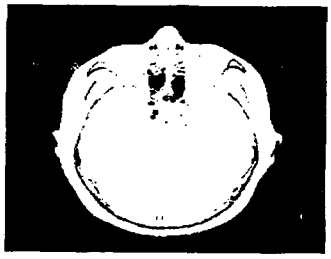

(b) The initial head mask produced using automatic thresholding by curve fitting.

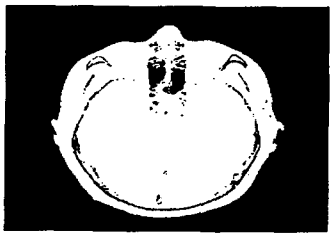

(c) Removing a background noise by morphological filtering.

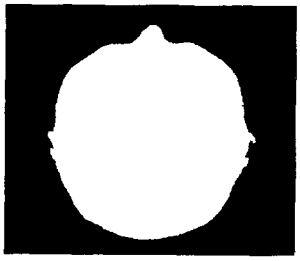

(d) The final head mask generated using boundary tracing and region filling.

2. Dual curve fitting

The brain region in the histogram of head MR images within the head masks is dominant as shown Fig. 4 because the brain region is larger than the other tissues in the MR images of the head. Brummer et. al.[4] generated an initial brain mask using automatic thresholding by curve fitting with a Gaussian curve to the histogram within the head mask.

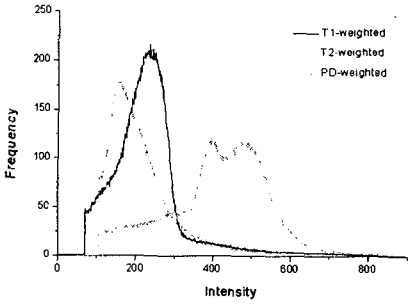

Fig. 4. Typical histograms of the MR images within the head masks.

But, fitting error can occur as shown in Fig. 5 because pixel distribution of the brain region in MR images may not have Gaussian distribution in many cases as shown in Fig. 4. Therefore, we try to achieve separately fitting with two Gaussian curves for the left and right side of the top-half of the histogram within the head masks. We call the fitting *a dual* curve fitting.

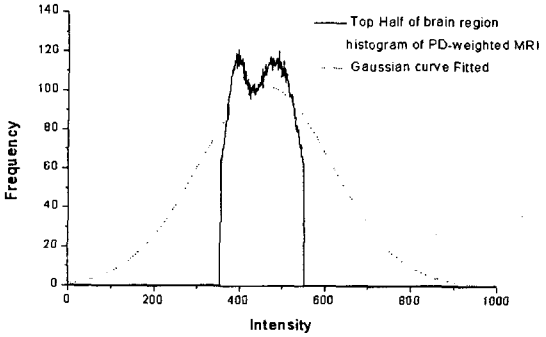

Fig. 5. Gaussian curve fitting with large error to the top-half of the histogram of PD-weighted images for automatic thresholding.

The dual curve fitting means that two Gaussian curves are independently fitted to two parts, the left and right part, of the histogram as shown in Fig. 7 and 8.

Initial brain masks are generated by automatic thresholding using the dual curve fitting to the histogram of MRI data sets within the head masks. For the fitting parts, the top-half[2] is selected from the histogram as shown in Fig. 6 and 7 (a), and the left part, $h_L(f)$, and the right part, $h_R(f)$, of the top-half histogram are chosen as shown in Fig. 7 (b).

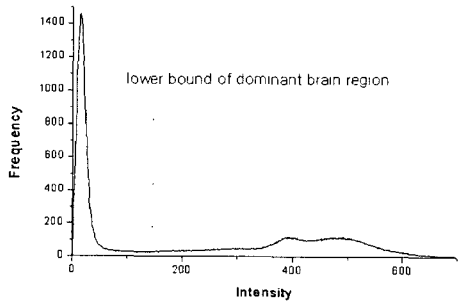

(a) Lower bound.

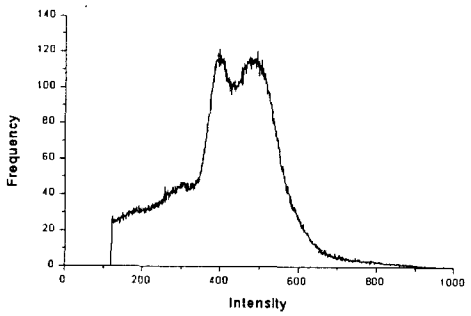

(b) the dominant brain region found in the histogram.

Fig. 6. Finding lower bound of the dominant brain region in the histogram of the MR images of the head for dual curve fitting.

To begin with, a dominant part, $h_b(f)$, of the histogram within the head masks is chosen like in Eq. (4) and Fig. 6 for a dual curve fitting with two Gaussian curves,

$$h_b(f) = \begin{cases} h(f), & f \geq f_{\min} \\ 0, & \text{otherwise} \end{cases} \tag{4}$$

where f_{min} is determined as Eq. (5), N is a range of pixel value, and T is a constant. The f_{min} means the position with minimum value of the histogram as shown in Fig. 6 (a).

```
for(i = f_max; i < N; i++) {
    flag_min = 1;
    for(j = i; j < i + T; j++) {
        if( h(i) > h(j) ) {
            flag_min = 0;
            break;
        }
    }
    if( flag_min ) {
        f_min = i;
        break;
    }
}
```

(5)

$$f_{\max} = \arg\max_{f} h(f) \tag{6}$$

The top-half of the histogram can be found as Eq. (7) and Fig. 7 (a) from the dominant part of the histogram extracted by Eq. (4),

$$h_{\max} = \max h_b(f),$$

$$h_t(f) = \begin{cases} h_b(f), & h_b(f) \geq h_{\max}/2 \\ 0, & \text{otherwise} \end{cases} \tag{7}$$

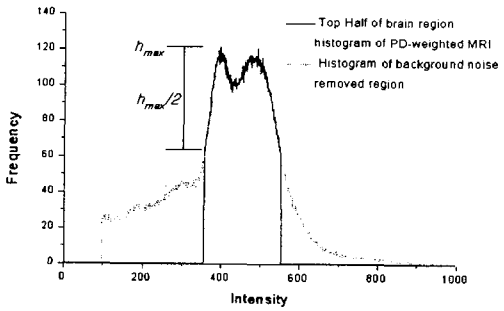

(a) The top-half

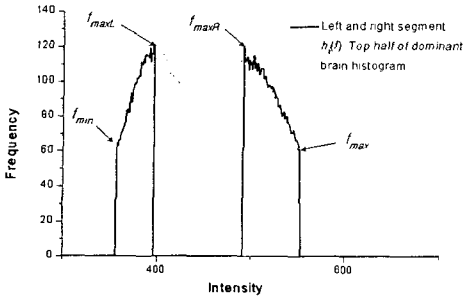

(b) the left and right curve selected.

Fig. 7. Selection of the left and right curve of the top-half of the histogram for dual curve fitting.

The left and right part, $h_L(f)$ and $h_R(f)$, of the top-half $h_t(f)$ of the histogram are determined by Eq. (8) as shown in Fig. 7 (b). The left and right part of the histogram range from f_{min} and f_{maxR} to f_{maxL} and f_{max}, respectively, as shown in Fig. 7 (b). The f_{min}, f_{max} are lowest and highest pixel value in the top-half histogram, respectively. The f_{maxL}, f_{maxR} are the first position with local maximum away from f_{min}, f_{max}, respectively. The left and right part of the histogram are selected as Eq. (8),

$$h_L(f) = \begin{cases} h(f), & f_{min} \le f \le f_{maxL} \\ 0, & \text{otherwise} \end{cases}$$

$$h_R(f) = \begin{cases} h(f), & f \ge f_{maxR} \text{ and } h(f) \ge h_{max}/8 \\ 0, & \text{otherwise} \end{cases} \quad (8)$$

where

$$f_{min} = \arg\min_f h_t(f) > 0$$

$$f_{max} = \arg\max_f h_t(f) > 0 \quad (9)$$

The dual curve fitting with two Gaussian curves to the left part $h_L(f)$ and the right part $h_R(f)$ extracted above can be achieved as shown in Fig. 8.

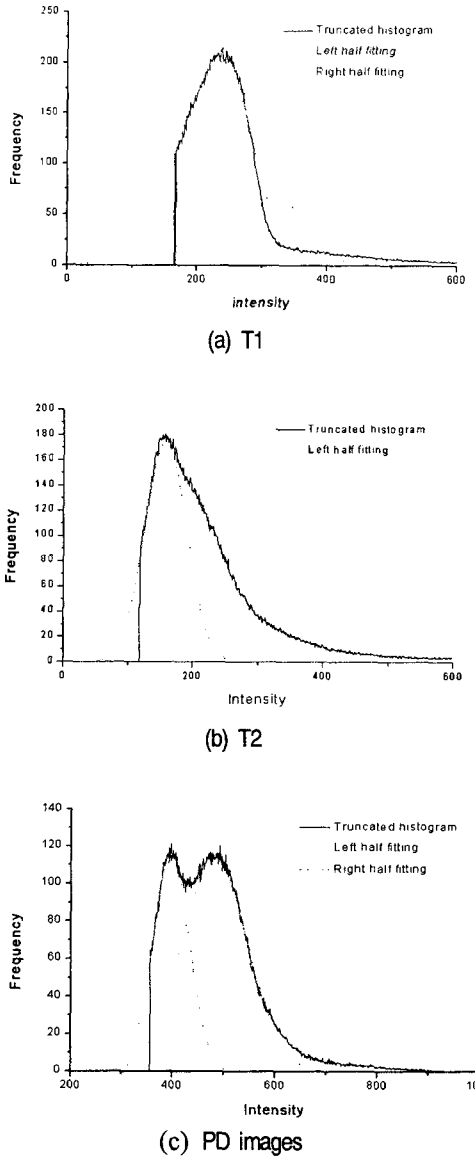

Fig. 8. Dual curve fitting, in which two Gaussian curves are used, to the top-half of the histogram of (a) T1, (b) T2, and (c) PD images.

The threshold levels depending on the degree of clustering are determined from two Gaussian curves fitted to the left and right part of the top-half of the histogram. In our case, the threshold levels are $f = \mu \pm 2\sigma$ within which the area under the fitted Gaussian curve of that range is 95.9%.

Table 1. Determinations of threshold levels to generate initial brain masks for T1, T2, PD, and SPGR MR images.

	T_L	T_R
T1-weighted	$\mu_L \quad 2\sigma_L$	$\mu_R + 2\sigma_R$
T2-weighted	$\mu_L \quad 2\sigma_L$	∞
PD-weighted	$\mu_L \quad 2\sigma_L$	$\mu_R + 2\sigma_R$
SPGR	$\mu_L \quad 2\sigma_L$	$\mu_R + 2\sigma_R$

The threshold levels for T1, T2, PD, and SPGR MR images are described in Table 1, where T_L, T_R are the left and right threshold level, μ_L, μ_R and σ_L, σ_R are mean values and standard deviations of the left and right Gaussian curve fitted to the top-half histogram, respectively, as shown in Fig. 8. The upper threshold is not used for T2-weighted MR images because the pixel values of gray matter are higher than the other tissues. The initial brain masks obtained by automatic thresholding using the dual curve fitting for T1, T2, PD, and SPGR MR images are shown in Fig. 9.

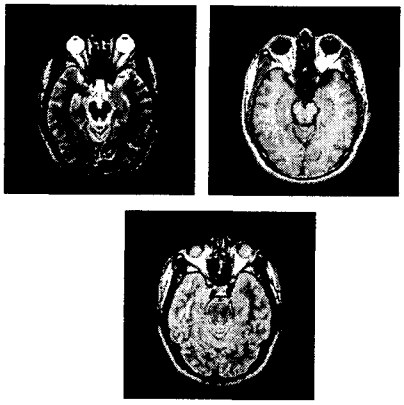

(a) Original images

(b) initial brain masks

Fig. 9. Generation of initial brain masks for T1-, T2- and PD-weighted image:

3. 3D morphological operations

In this paper, 2D morphological operations like erosion, dilation[9], labeling of connected- components[4], and max-feature operation[4] are extended to 3D operations to separate slightly connected regions in the initial brain masks obtained in the previous step. The 3D morphological operations are applied to *a cubic volume* of masks, as shown in Fig. 10 (b), generated by interpolation from the initial brain masks, as shown in Fig. 10 (a), because the thickness between the initial brain masks is large. The cubic volume of masks consisting of cubic voxels can be achieved by applying cubic interpolation function R_c at the range of $0 \le |x| \le 2$ like Eq. (10)[8],[9],

$$R_c = \begin{cases} (a+2)|x|^3 - (a+3)|x|^2 + 1, & 0 \le |x| \le 1 \\ a|x|^3 - 5a|x|^2 + 8a|x| - 4a, & 1 \le |x| \le 2 \end{cases} \quad (10),$$

where weighting factor $a=-1/2$ proposed by Keys[8].

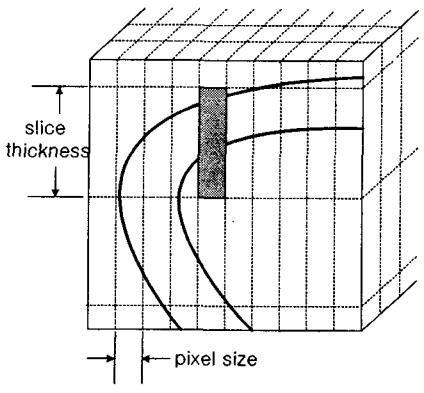

(a) Errors in 3D morphological operations or in

application of Brummer's method to a volume of MR images clinically used may be occurred because the slice thickness between masks is larger than pixel size. Morphological operations in Brummer's method[4] is achieved in 2D to perform the overlap test for generating 3D volume of masks.

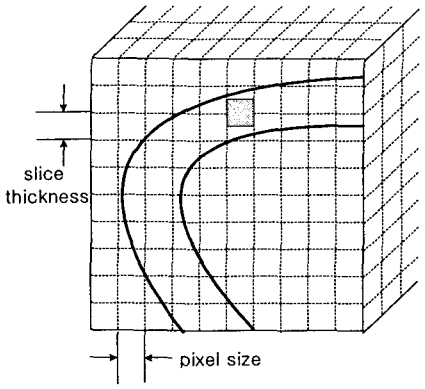

(b) Our 3D morphological operations in the cubic volume of masks can overcome errors introduced by the overlap test of Brummer's method because the volume of masks consists of cubic voxels.

Fig. 10. Segmentation in the volume of masks according to slice thickness:

Errors in 3D morphological operations or in application of Brummer's method[4] to a volume of MR images clinically used may be occurred because the slice thickness between masks is much larger than pixel size as shown in Fig. 10 (a). Morphological operations in Brummer's method[4] is achieved in 2D to perform the overlap test for generating 3D volume of masks. Our 3D morphological operations in the cubic volume of masks can overcome errors introduced by the overlap test of Brummer's method because the volume of masks consists of cubic voxels as shown in Fig. 10 (b).

Fig. 11. (b) represents the cubic volume of masks with the size of 256×256×256 generated from the volume of the initial brain masks with the size of 256×256×20. The procedure of the 3D morphological operations applied to the cubic volume of masks for extracting the brain region is as follows: erosion(Fig. 11 (c)), labeling of the connected-components, max-feature operation(Fig. 11 (d)), and dilation (Fig. 11 (e)) in a sequence. The erosion and dilation of N_{morph} iterations are applied to the cubic volume of masks. After labeling of the connected-components is applied to the cubic volume of masks eroded by N_{morph} operations, max-feature operation[4] is applied to the cubic volume of masks to select the largest volume of the connected-components labeled in above process. The max-feature operation means a selection of the largest connected-component in the labeled cubic volumes, in which the max-feature is the brain region in our case. The dilations of N_{morph} iterations are applied to the volume of masks selected by the max-feature operation. Fig. 11 (c) and (e) depicts the cubic volume of masks applied with 3D morphological erosion and dilation(N_{morph}=4), respectively. Fig. 11 (d) is the largest volume of masks selected using the max-feature operation after labeling of connected-components. Fig. 11 (f) represents the corresponding slice extracted from the cubic volume of masks of Fig. 11 (e).

(a) initial brain mask

(b) reconstructed cubic volume of masks

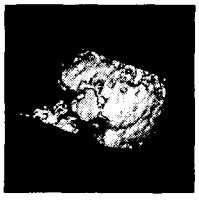

(c) 3D morphologically eroded volume(Nmorph=4)

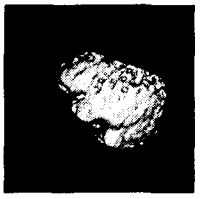

(d) the largest volume after labeling of connected-components in 3D

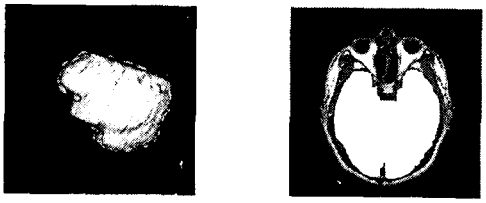

(e) 3D morphologically dilated volume(Nmorph=4).

(f) intermediate brain mask depicted in white region.

Fig. 11. Generation of intermediate brain masks:

Operation kernel of 3×3×3 is used for 3D morphological erosion and dilation operations, in which the parameter of N_{morph} is empirically determined and typically N_{morph}=4. In a case of the connection between brain and skull with blood vessels, the part can be separated by increasing the parameter of N_{morph}. But, higher N_{morph} can distort the brain region. The parameter of N_{morph}=4 will be good choice in 3D erosions and dilations for extracting the brain region of MR images.

In morphological operations, thresholding by the dual curve fitting(TDCF) can be adapted to the images within the volume of masks for refinement in intermediate segmentation stage. For example, TDCF can be used, after each erosion or dilation operation, or before each labeling and max-feature operation, as shown in Fig. 12, in which TDCF in erosions provided better separation between brain and skull.

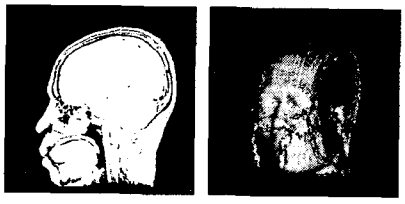

(a) initial brain mask, and results after

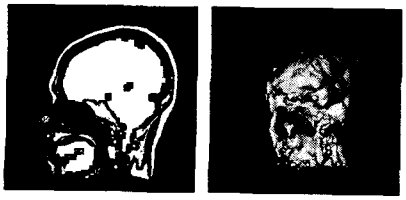

(b) 4 erosion operations without TDCF

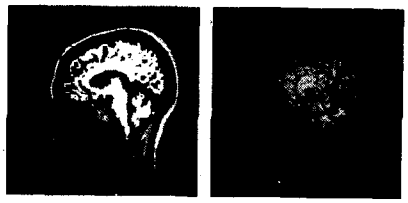

(c) 4 erosion and TDCF operations, followed by labeling of the connected components and max-feature operation.

Fig. 12. TDCF in erosions(Nmorph=4) provides better separation between brain and skull(left: 2D view, right: 3D view):

If there is connection between brain and skull with blood vessels after morphological operations, the part can be easily separated by manually editing one or two slices at the step of erosion. The manual editing, labeling of the connected components, and max-feature operation are repeatedly applied until nonbrain region is deleted, where labeling of the connected components and max-feature *operation are to check separation of the part for reducing* user's labor in manual editing as shown in Fig. 13.

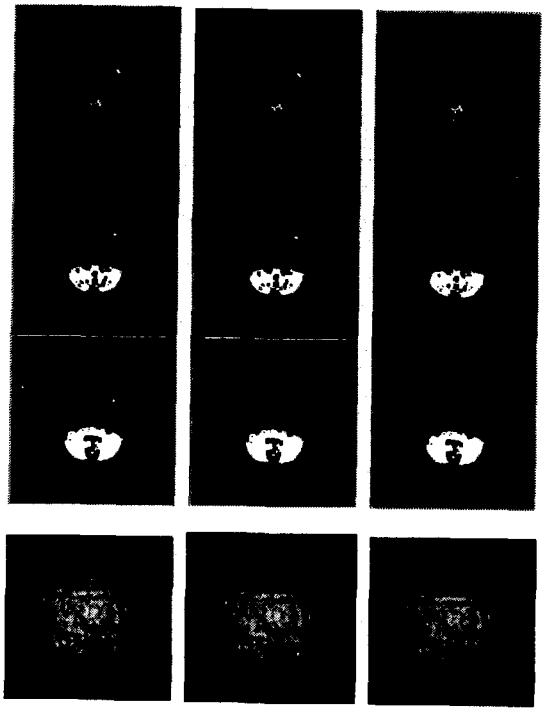

(a) (b) (c)

Fig. 13. The connection between brain and skull after erosions(Nmorph=4) can be easily separated by manually editing one or two slices at the step of erosion. The manual editing, labeling of the connected components, and max-feature operation are repeatedly applied until nonbrain region is deleted, where labeling of the connected components and max-feature operation are to check separation of the part for reducing user's effort in manual editing.
(a) The connection after erosions was
(b) separated by deleting small blob only in the third window among three slices(top three windows) in a sequence.
(c) The separated nonbrain region was deleted by labeling of the connected components and max-feature operation. Each volume of masks was displayed in rendering at the bottom window.

Manual editing is performed on the 2D display window of left side in Fig. 14 and its result is viewed on the 3D display window of right side in Fig. 14.

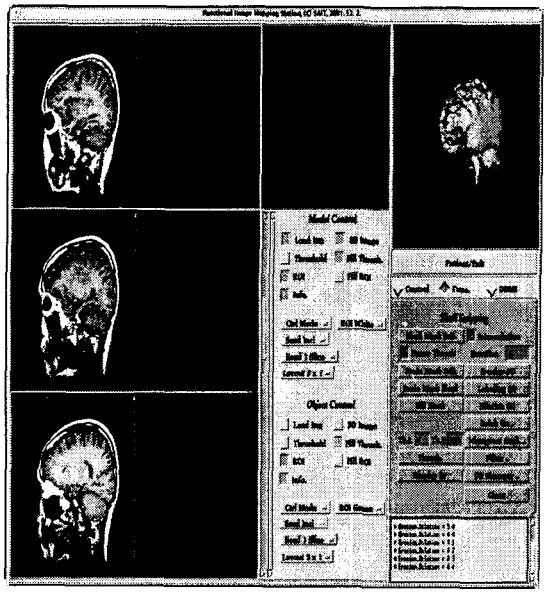

Fig. 14. This is our software module, which has display windows and control or option buttons, for automatic segmentation of a brain region in MR mages using automatic thresholding and 3D morphological operations. Three windows of left side are to display original images and masks in 2D, and are to perform manual editing. Head or brain masks are displayed on the window of right side in 3D.

The 3D morphological operations applied to the cubic volume of masks for automatic segmentation of the brain region in head MR images do not require a specific displayed type of slices and do not require the MRI data sets to contain the entire brain.

4. Mask refinement

The final brain masks are generated by automatic thresholding using the dual curve fitting to the top-half of the histogram of the regions within the cubic volume of masks extracted by the 3D morphological operations. This procedure can remove nonbrain regions included in process of the 3D morphological operations.

The dual curve fitting and 3D morphological operations described in above section are again applied to separate brain regions slightly connected to the skull or to remove nonbrain regions. The cubic volume of brain masks after applied with morphological operations in the generation step of intermediate brain masks contains nonbrain regions as shown in Fig. 15 (a).

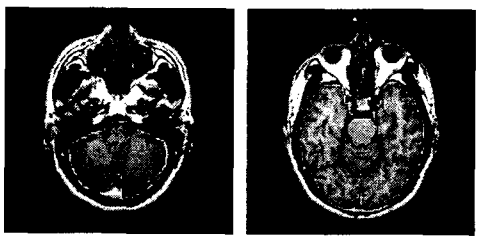

(a)

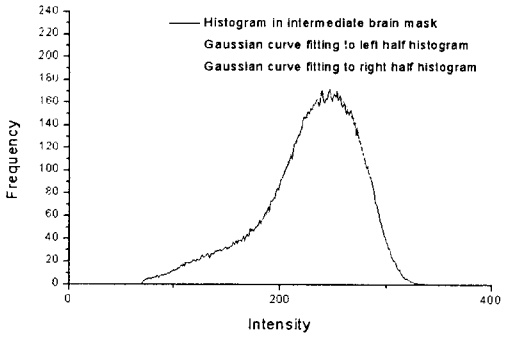

(b)

Fig. 15. (a) Intermediate brain masks depicted in a white curve as a mask boundary, and (b) the histogram of the MR images within the intermediate masks and two Gaussian curves fitted by the dual curve fitting method.

The procedure of the mask refinement erases nonbrain regions and fills the holes in the masks. Nonbrain regions within the volume of masks are erased by automatic thresholding and the 3D morphological operations because the cubic volume of masks contains most of the brain region as shown in Fig. 15 (b). Thresholding is automatically achieved by the dual curve fitting to the top-half of the histogram of regions within the volume of masks. The 3D morphological operations of N_{morph}=1~2 are applied to the volume of masks. The holes in the masks are filled using boundary tracing and region filling technique[9] as shown in Fig. 16.

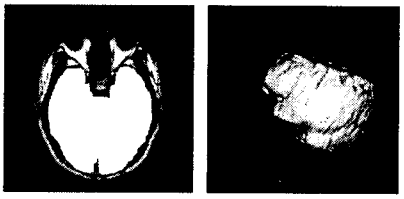

(a) The intermediate brain mask.

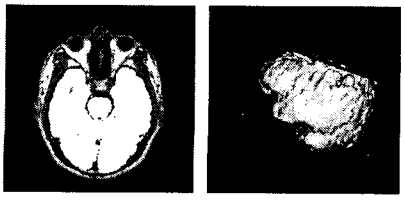

(b) the mask after automatic thresholding.

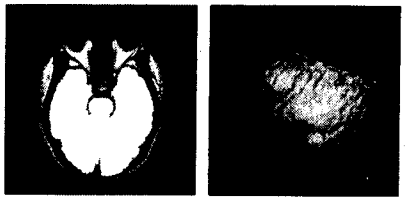

(c) boundary tracing and region filling.

Fig. 16. Generation of the final brain mask:

Table 2. MR images used in the experiments.

	pixel size	slice thickness	TE	TR
T1-weighted	0.82 mm	7.00 mm	12 ms	500 ms
T2-weighted	0.82 mm	7.00 mm	102 ms	3733 ms
PD-weighted	0.82 mm	7.00 mm	17 ms	3733 ms
SPGR	0.86 mm	1.5 mm	3500 ms	14500 ms

III. Experimental Results

Our algorithm for automatic segmentation of a brain region was implemented, as shown in Fig. 14, using C language, X Window System, and Motif library under UNIX environment on the SUN UltraSPARC II workstation. The method was applied to segment a brain region in SPGR, T1, T2, and PD MR images of human heads. MR images for experiments were acquired on GE 1.5 Tesla Signa scanner in steady state with typical parameters as shown in Table 2. T1, T2, and PD MR images, which are the image size of 256×256 with 20 slices, are usually clinically used for diagnosis of patients in hospital. A set of SPGR MR images consists of about 120 slices.

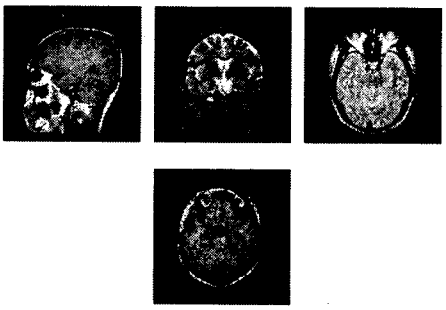

(a) Original images(sagittal T1-weighted, coronal T2 - weighted, axial PD-weighted, and axial SPGR MR image)

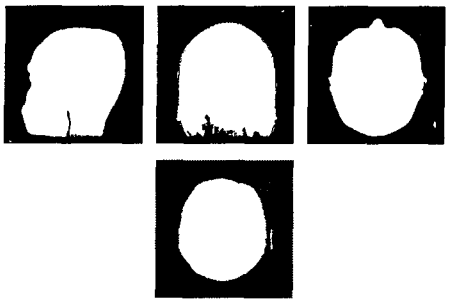

(b) head masks.

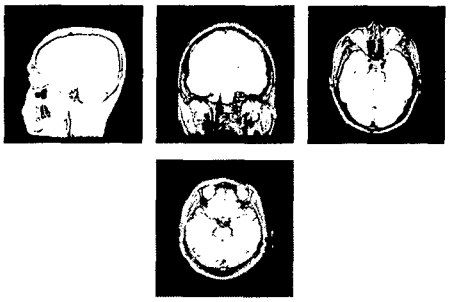

(c) initial brain masks.

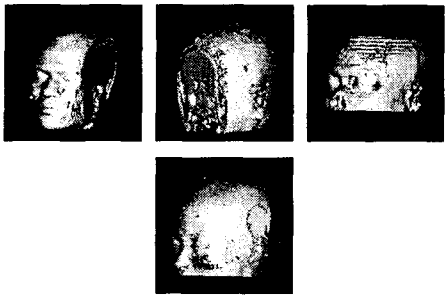

(d) cubic volumes of masks reconstructed from initial brain masks.

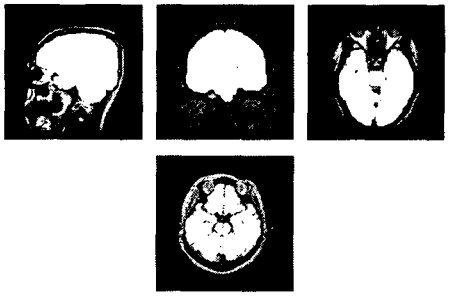

(e) intermediate brain masks.

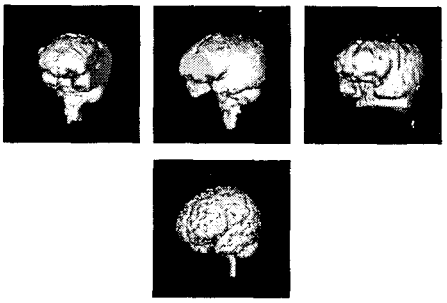

(f) volumes of masks reconstructed from intermediate brain masks.

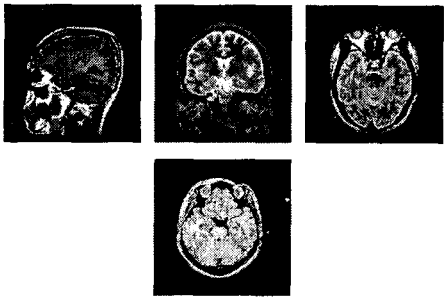

(g) final brain masks.

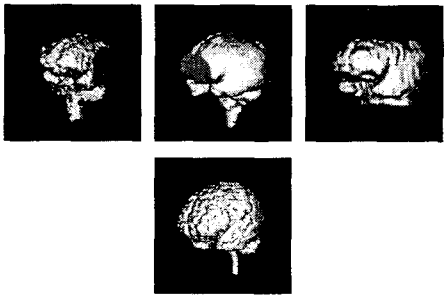

(h) volumes of masks reconstructed from final brain masks.

Fig. 17. *Segmentation of a brain region in MR images of a head by the proposed method.*

The brain masks generated by our method for coronal, sagittal, and axial MR images are shown in Fig. 17. Fig. 17 (a) represents sagittal T1, coronal T2, axial PD, and axial SPGR MR image, respectively. Fig. 17 (b),(c),(e),and (g) depicts head masks, thresholded brain masks,

morphologically operated masks, and refined masks, respectively. Fig. 17 (d),(f), and (h) are volume rendered images of the volume of masks generated from each steps. The head masks were achieved by automatic thresholding using curve fitting with Rayleigh curve to the histogram. The cubic volume of masks reconstructed using the cubic interpolation functions consists of $256\times256\times256$ voxels with 8 bits per voxel. The kernel used in 3D morphological operations was the size of $3\times3\times3$. Mask refinement was achieved by again applying the dual curve fitting and the 3D morphological operations to the volume of images within the volume of intermediate masks to erase nonbrain regions obtained in the previous 3D morphological operations.

Quantitative comparisons of segmentation results were measured by Zijdenbos[13]'s similarity index S represented as Eq. (11) in which A_1 and A_2 are two binary images, respectively, and $S\in[0\sim1]$.

$$S=2\frac{|A_1\cap A_2|}{|A_1|+|A_2|} \tag{11}$$

Results segmented by the proposed method were compared with the brain regions manually drawn by clinical experts. Comparisons for three orthogonally displayed image sets of T2 MR images showed that the proposed method could be applied to any displayed type of MR images and could well segment extreme slices of image sets as shown in Fig. 18 (a).

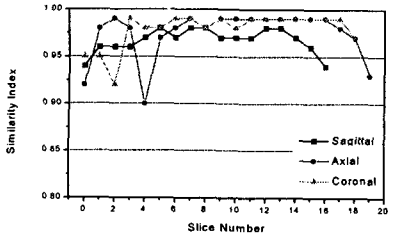

(a) For coronal, sagittal, and axial T2-weighted images.

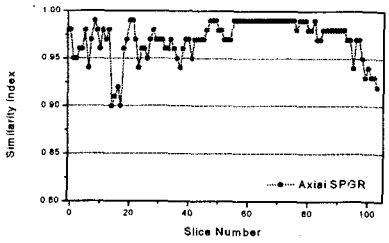

(b) for axial SPGR images.

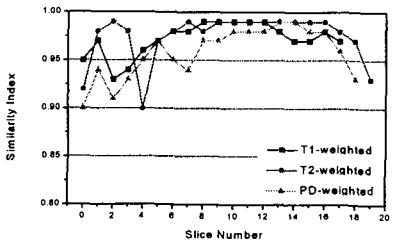

(c) for axial T1-, T2-, and PD-weighted images.

The slice number increases from left to right, from back to front, and from bottom to top in the head. The approximate position of each slice in this figure can be found at each volume of masks in Fig. 17.

Fig 18. Comparisons, in similarity index, of the brain regions segmented by our method with manually drawn images in MR images of a head.

Segmentation results by our method for axial SPGR, T1, T2, and PD MR images were compared with brain regions manually drawn by clinical experts in similarity index, and provided over 0.95 of similarity index for the images as shown in Fig. 18 (b) and (c). Comparisons of the brain regions segmented by our method with manually segmented brain regions for 20 sets of MR images were shown over 0.97 of similarity index as shown in Table 3. The execution time is within 3 minutes on the SUN UltraSPARC II workstation. Nonbrain regions obtained in automatic segmentation can be manually edited in morphological operation or mask refinement stage. Manual

editing in the stage of 3D morphological operations can be achieved with less effort than in mask refinement stage because mouse operations for editing in the morphological stage is less often than in the mask *refinement stage.*

Table 3. Comparisons, in similarity index, of the brain regions segmented by our method with manually drawn images in 20 sets of MR images of a head.

	Similarity Index
T1-weighted	0.972±0.005
T2-weighted	0.978±0.006
PD-weighted	0.975±0.004
SPGR	0.977±0.005

IV. Conclusion

We proposed a novel technique for automatic segmentation of a brain region in single channel MR images for visualization and analysis of a human brain. In the method, the brain region is segmented by automatic thresholding using the dual curve fitting and by 3D morphological operations in a cubic volume of masks reconstructed from thresholded images. The dual curve fitting can reduce an error in curve fitting to the histogram of MR images. The 3D morphological operations, including erosion, labeling of connected-components, max-feature operation, and dilation, were applied to the cubic volume of masks reconstructed from the thresholded brain masks. This method can automatically segment the brain region in any displayed type of sequences, including extreme slices, of SPGR, T1-, T2-, and PD-weighted MR image data sets which are not required to contain the entire brain. In the experiment, comparisons of the brain regions segmented by our method with manually segmented brain regions for 20 sets of coronally, sagittally, and axially displayed T1, T2, PD, and SPGR MR images were shown over 0.97 of similarity index. This showed our method will be a useful technique to segment a brain region in the MR images for visualization and analysis.

References

[1] P. A. Freeborough and N. C. Fox, "Assessing Patterns and Rates of Brain Atrophy by Serial MRI: A Segmentation, Registration, Display and Quantification Procedure", Proc. Visualization in Biomedical Computing '96, Vol.1131, pp.419~428, 1996.

[2] B. Johnston, M. S. Atkins, B. Mackiewich, and M. Anderson, "Segmentation of Multiple Sclerosis Lesions in Intensity Corrected Multispectral MRI", IEEE Trans. Medical Imaging, Vol.15, pp.154-169, 1996.

[3] G. B. Aboutanos and B. M. Dawant, "Automatic Brain Segmentation and Validation: Image-based Versus Atlas-based Deformable Models", Proc. SPIE-Medical Imaging 1997, Vol.3034, pp.299-310, 1997.

[4] Marijn E. Brummer, Russell M. Mersereau, Robert L. Eisner, and Richard R. J. Lewine, "Automatic Detection of Brain Contours in MRI Data Sets", IEEE Trans. Medical Imaging, Vol.12, pp.153-166, 1993.

[5] M. Stella Atkins and Blair T. Mackiewich, "Fully Automatic Segmentation of the Brain in MRI", IEEE Trans. Medical Imaging, Vol.17, pp.98-107, 1998.

[6] J. W. Snell, M. B. Merickel, J. M. Ortega, J. C. Goble, J. R. Brookeman, and N. F. Kassell, Segmentation of the Brain from 3D MRI using a Hierarchical Active Surface Template, Proc. SPIE, Vol.2167, pp.2-9, 1994.

[7] J. Ashburner and K. J. Friston, "Multimodal Image Coregistration and Partitioning - a Unified Framework", NeuroImage, 6(3):209-217, 1997.

[8] R. G. Keys, "Cubic Convolution Interpolation for Digital Image Processing", IEEE Trans. Acoustics, Speech, and Signal Processing, AASP-29, 6, pp.1153-1160, 1981.

[9] William K. Pratt, Digital Image Processing, 1991.

[10] W. H. Press, B. P. Flannery, Saul A. Teukolsky, William T. Vetterling, Numerical Recipes in C, Cambridge University Press, Cambridge, 1988.

[11] W. A. Edelstein, P. A. Bottomley, and L. M. Pfeifer,

"A Signal-to-noise Calibration Procedure for NMR Imaging Systems", Med. Phys., Vol.11, pp.180-185, 1984.

[12] M. Henkelman, "Measurement of Signal Intensities in the Presence of Noise in MR Images", Med. Phys., Vol.12, pp.232-233, 1985.

[13] Alex P. Zijdenbos, Benoit M. Dawant, Richard A. Margolin, and Andrew C. Palmer, "Morphometric Analysis of White Matter Lesions in MR Images: Method and Validation", IEEE Trans. Medical Imaging, Vol.13, pp.716-724, 1994.

조 동 욱 (Dong-Uk Cho) 정회원

1983년 2월 : 한양대 공대 전자공학과 (공학사)

1985년 9월 : 한양대 대학원 전자공학과 (공학석사)

1989년 2월 : 한양대 대학원 전자통신공학과 (공학박사)

2000년 3월 ~ 현재 : 충북과학대 정보통신공학과 교수

<관심분야> : 영상처리 및 인식, 생체측정, ITS, 정보보호, 퍼지이론

김 태 우(Tae-Woo Kim) 정회원

1990년 : 한양대학교 전자통신공학과 졸업(학사)

1992년 : 한양대학교 대학원 전자통신공학과(공학석사)

1995년 : 한양대학교 대학원 전자통신공학과(공학박사)

1995년 ~ 1997년 : 한양대학교 산업과학연구소 선임연구원

1997년 ~ 현재 : 삼성종합기술원 메디컬응용팀 책임연구원

<관심분야> : 영상처리, 인공 신경망, 생체신호처리, 영상복합화, 뇌지도화 등

신 승 수(Seung-Soo Shin) 종신회원

2001년 2월 : 충북대학교 대학원 (이학박사)

현재 : (주)시그마정보기술 연구소장

<관심분야> : 이미지프로세싱, 의료정보, 영상통신, ATM, 트래픽공학